Research Article Vol. 29, No. 3 / 1 February 2021 / *Optics Express* 4147

Optics EXPRESS

Highly sensitive hydrogen sensor based on an in-fiber Mach-Zehnder interferometer with polymer infiltration and Pt-loaded WO_3 coating

BIN DU,[1,2] JUN HE,[1,2,*] MINGHONG YANG,[3] YING WANG,[1,2] XIZHEN XU,[1,2] JIACHEN WANG,[1] ZHE ZHANG,[1,2] FENGCHAN ZHANG,[1,2] KUIKUI GUO,[1,2] AND YIPING WANG[1,2]

[1] *Key Laboratory of Optoelectronic Devices and Systems of Ministry of Education/Guangdong Province, College of Physics and Optoelectronic Engineering, Shenzhen University, Shenzhen 518060, China*
[2] *Shenzhen Key Laboratory of Photonic Devices and Sensing Systems for Internet of Things, Guangdong and Hong Kong Joint Research Centre for Optical Fibre Sensors, Shenzhen University, Shenzhen 518060, China*
[3] *China National Engineering Laboratory for Fiber Optic Sensing Technology, Wuhan University of Technology, Wuhan 430070, China*
[*] *hejun07@szu.edu.cn*

Abstract: A highly sensitive fiberized hydrogen sensor based upon Mach-Zehnder interference (MZI) is experimentally demonstrated. The hydrogen sensor consists of an MZI realized by creating an air cavity inside the core of a half-pitch graded-index fiber (GIF) by use of femtosecond laser micromachining. Thermosensitive polymer was filled into the air cavity and cured by UV illumination. Subsequently, the external surface of the polymer-filled MZI was coated with Pt-loaded tungsten trioxide (WO_3). The exothermic reaction occurs as Pt-loaded WO_3 contacts the target of the sensing, i.e. hydrogen in the atmosphere, which leads to a significant local temperature rise on the external surface of the coated MZI sensor. The sensor exhibits a maximum sensitivity up to -1948.68 nm/% (vol %), when the hydrogen concentration increases from 0% to 0.8% at room temperature. Moreover, the sensor exhibits a rapid rising response time (hydrogen concentration increasing) of ~38 s and falling response time (hydrogen concentration decreasing) of ~15 s, respectively. Thanks to its small size, strong robustness, high accuracy and repeatability, the proposed in-fiber MZI hydrogen sensor will be a promising tool for hydrogen leakage tracing in many areas, such as safety production and hydrogen medical treatment.

1. Introduction

Hydrogen plays a significant role in the modern society in a wide range of fields, such as aerospace, chemical industry, and medical treatment, either as the fuel, raw material or even medicine [1,2]. The massive applications bring about serious concern over the issue of safety. As a highly inflammable and explosive gas, the leakage of hydrogen can result in catastrophic incidents [2]. Consequently, high-sensitivity hydrogen sensors are strongly desired. In recent years, fiber-optic hydrogen sensors attract great attention for hydrogen leakage tracing, owning to their unique advantage on resistance to electromagnetic interference (EMI) over conventional electronic hydrogen sensors. Among these fiber hydrogen sensors, two main sensitive materials are utilized, i.e., Palladium (Pd) [1,3–9] and Platinum (Pt)-loaded tungsten oxide (WO_3) [10–15]. Pd can absorb a large number of hydrogen molecules, leading to a volume expansion for several hundreds of times and a change in the refractive index (RI) [1,3–9]. For example, in 2014, Wang et al. reported a hydrogen sensor based on a Pd-coated in-fiber Mach-Zehnder interferometer (MZI), which exhibited a sensitivity of ~70 pm/% within a range of 0~8% (vol %) [3]. In 2015, Gu et al. illustrated a hydrogen sensor based on a microfiber MZI using Pd/Au nanowire as a plasmonic waveguide, and they achieved hydrogen detection in a wide concentration range of

#417424 https://doi.org/10.1364/OE.417424
Journal © 2021 Received 14 Dec 2020; revised 16 Jan 2021; accepted 18 Jan 2021; published 25 Jan 2021

0~20% [4]. In general, the Pd-based fiber hydrogen sensors always have compact size. However, the Pd film could easily be oxidized by the oxygen in the atmosphere, and these types of hydrogen sensors typically have a low sensitivity of less than 1 nm/% [16].

Pt-loaded WO_3 is another important functional material for hydrogen sensing [10–15]. It can dissociate hydrogen molecule into atoms and decrease the reaction activation energy. Exothermic reaction will occur when Pt-loaded WO_3 contacts with hydrogen in the atmosphere. Heat will be released during the exothermic reaction and could be detected by temperature sensors. Hence, various in-fiber hydrogen sensors based on Pt-loaded WO_3 coatings have been proposed. For instance, in 2012, Yang et al. reported a hydrogen sensor based on a fiber Bragg grating (FBG) with Pt-loaded WO_3 coatings [10]. The coated-FBG hydrogen sensor exhibited a wavelength shift of ~ 140 pm in case the hydrogen concentration was increased from 0% to 4%. Subsequently, in 2014, Wang et al. reported a hydrogen sensor based on a selectively infiltrated photonic crystal fiber (PCF) with Pt-loaded WO_3 coatings [11]. They achieved a high sensitivity of 32.3 nm/% within the range of 1~4% H_2 in the air. However, this type sensor could only be used for detecting hydrogen with a relatively high concentration of beyond 1%. Then, in 2016, Xu et al. demonstrated a hydrogen sensor based on a fiber Sagnac interferometer coated with Pt-loaded WO_3/SiO_2 layer and achieved a sensitivity of -7.877 nm/% in the range of 0 ~ 1% [17]. However, the sensor features a larger size since a section of coated highly birefringent fiber with a length of a few centimeters is required to construct the Sagnac interferometer. Moreover, in 2018, Li et al. reported a hydrogen sensor based on a PDMS-formed fiber Fabry-Perot interferometer (FPI) with Pt-loaded WO_3/SiO_2 embedded on the external surface of the FPI [12]. This type sensor exhibits a sensitivity of -15.14 nm/% within the hydrogen concentration range of 0 ~ 1%. To the best of our knowledge, the highest hydrogen sensitivity of the fiber hydrogen sensors reported at present is 32.3 nm/%, which was achieved in a selectively infiltrated PCF with a high temperature sensitivity of –7.69 nm/°C [11]. Recently, we developed a highly sensitive temperature sensor based on a UV-curable polymer-filled MZI created in graded index fiber [18]. An extremely high temperature sensitivity of −13.27 nm/°C was achieved. This highly sensitive MZI temperature sensor could potentially be developed for trace hydrogen detection by coating these MZI temperature sensors with hydrogen sensitive Pt-loaded WO_3 powder.

In this paper, a miniaturized and highly sensitive fiber MZI hydrogen sensor based on thermosensitive polymer infiltration and Pt-loaded WO_3 coating, is experimentally demonstrated. The MZI is formed by femtosecond laser-drilled micro-air-cavity in the core of a graded-index fiber (GIF) spliced with two single-mode fibers (SMFs). The micro-air-cavity is then filled with thermosensitive UV-curable polymer, and the external surface of the filled-MZI is coated with Pt-loaded WO_3 powder. The half-pitch GIF could enlarge the optical mode area, and hence decreases the insertion loss and increases the fringe visibility of the MZI. In addition, the employment of the half-pitch GIF could also reduce the difficulty in the ablating and filling process for fabricating the MZI. The thermosensitive polymer-filled and Pt-loaded WO_3-coated fiber MZI exhibits a maximum sensitivity of -1948.68 nm/% to hydrogen in a low concentration range of 0 ~ 0.8%. A rising response time (hydrogen concentration increases from 0% to 0.8%) of ~ 38 s and a falling response time (hydrogen concentration decreases from 0.8% to 0%) of 15 s are obtained in the air at room temperatures, respectively. These characteristics make the proposed in-fiber MZI hydrogen sensor suitable for monitoring hydrogen leakage in many fields, such as safety production and hydrogen medical treatment.

2. Hydrogen sensing mechanism

The schematic of the proposed in-fiber MZI hydrogen sensor is shown in Fig. 1. A half-pitch (L_{GIF} = 490 μm) GIF serves as a pair of collimators between which an air cavity is created in one lateral side of the GIF by means of femtosecond laser micromachining. The air cavity is filled with thermosensitive polymer, which is cured by use of UV illumination. Then, the external surface of the polymer-filled MZI is coated with Pt-loaded WO_3 powder.

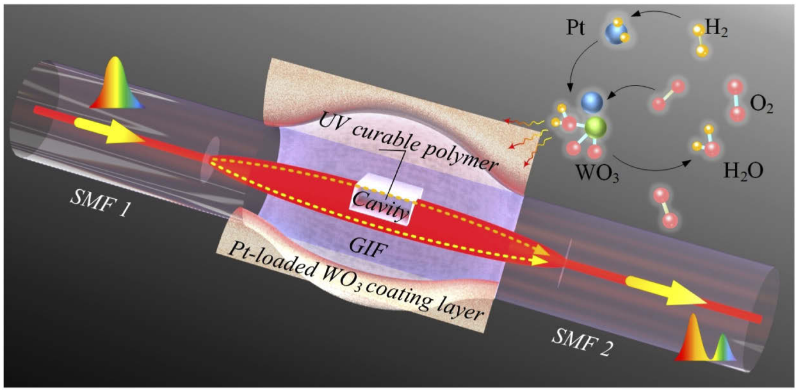

Fig. 1. The schematic of the structure and sensing mechanism of the in-fiber MZI hydrogen sensor. (SMF: single mode fiber, GIF: graded index fiber, Pt: platinum, WO_3: tungsten oxide.)

An optical probe beam is sent into the sensor through a lead-in SMF (i.e., SMF1 in Fig. 1). When light transmits in the GIF, the radial beam waist (ω_{GIF}) gets larger at a longer transmission distance, and reaches its maximum (~20 µm) at the GIF quarter-pitch position (i.e. at a distance of ~245 µm, where the air cavity is created) [18–20]. A cavity width larger than ω_{GIF} could enable easier infiltration of UV-curable polymer into the cavity and avoid the formation of air bubbles in the infiltrated cavity. Hence, a cavity width of 30 µm was chosen for sensor fabrication. On the other hand, it is obvious a larger ω_{GIF} can significantly reduce the precision requirement in the laser ablating process for fabricating the air cavity and reduce the difficulty in filling the UV-curable polymer. As a result, one part of the input beam transmits through the polymer-filled cavity, whereas the other part propagates in the remained GIF core. A lead-out SMF (i.e. SMF2 in Fig. 1) is connected to the output end of the half-pitch GIF, at which two optical beams recombine and interfere with each other. The indices of the remained GIF core and the cured polymer are different (i.e., 1.491 and 1.540, respectively), leading to an optical path difference in the MZI.

The light intensity can be expressed as [18]

$$I_{out} = I_{polymer} + I_{GIF} + 2\sqrt{I_{polymer} I_{GIF}} \cos(2\pi L_C \Delta n / \lambda + f_0)\,, \tag{1}$$

where Δn is the refractive index difference between the UV-curable polymer ($n_{polymer}$) and GIF core (n_{GIF}), L_c is the cavity length, and ϕ_0 is the initial phase difference. Note that the initial phase difference f_0 could be ignored in Eq. (1). The resonance dip wavelength (λ_m), defined as the m^{th} order interference dip, can be expressed as [18]

$$\lambda_m = 2L_C/(2m+1) \cdot \Delta n. \tag{2}$$

The temperature response of the proposed SMF-GIF-SMF MZI structure can be obtained as [21]

$$d\lambda/dT = \lambda_m/\Delta n \cdot (\alpha_P - \alpha_G). \tag{3}$$

Where α_P and α_G are the thermo-optic coefficients of the UV-curable polymer and silica, respectively. It should be noted that the UV-curable polymer has a much larger thermo-optic coefficient (α_P =~10^{-4}°C^{-1}) than that of silica (α_G=~10^{-6}°C^{-1}) [18,21,22]. Hence, wavelength shifts induced by temperature changes in α_G could be neglected, and a simplified relationship between the wavelength shift and α_P is obtained as

$$d\lambda/dT = \lambda_m/\Delta n \cdot \alpha_P. \tag{4}$$

It could be calculated from Eq. (2) that the same resonant wavelength at ~1568 nm is obtained for cavity length L_c of 48, 80, and 112 µm, at different orders of $m = 1$, 2, and 3, respectively. A shorter cavity length can lead to a large free spectral range (FSR), and hence the resonant wavelength tends to drift out of the light source bandwidth. However, a longer cavity length leads to an increase in transmission loss. Moreover, it could be seen from Eq. (4) that the temperature sensitivity is irrelevant to cavity length. As a result, a cavity length L_c of 80 µm was used in the sensor fabrication process.

The hydrogen sensing mechanism of the proposed MZI sensor is also illustrated in Fig. 1. Exothermic reaction will occur when Pt-loaded WO_3 coating material contacts with hydrogen in the atmosphere. These chemical reactions can be expressed as [11]

$$WO_3 + xH_2 \xrightarrow{Pt} WO_{3-x} \cdot xH_2O, \tag{5}$$

$$WO_{3-x} \cdot xH_2O + \frac{x}{2}O_2 \xrightarrow{Pt} WO_3 + xH_2O. \tag{6}$$

At first, H_2 molecules are absorbed by WO_3, leading to the formation of $WO_{3-x}{\cdot}H_2O$. Then, $WO_{3-x}{\cdot}H_2O$ reacts with the oxygen in the atmosphere, producing WO_3 and H_2O. Pt plays as catalyst in the chemical reaction, and a large amount of heat is generated during this process. As a result, the local temperature will increase, resulting in a change in the refractive index (RI) of the UV-curable polymer filled in the cavity. According to Eq. (4), the resonance dip wavelength (λ_m) in the interference spectrum will shift significantly since the UV-curable polymer has a large thermo-optic coefficient. Thus, the H_2 concentration can be determined by tracing the wavelength shift of λ_m.

3. Device fabrication

3.1. Preparation and characterization of Pt-loaded WO_3 powder

The Pt-loaded WO_3 powder used for hydrogen sensing in this work was prepared via sol-gel method [10,11]. At first, aqueous sol-gel of H_2WO_4 was obtained from 50 mL 0.5 mol/L Na_2WO_4 solution with cation-exchange resin, and then washed and centrifuged for 15 times with de-ionized water. After purification, the sol-gel was smashed by ultrasonic-vibrating. Subsequently, the sol-gel was mixed with 1.5 g $H_2PtCl_6{\bullet}6H_2O$ and stirred by magnetic stirrer at 80°C for 6 hours. The Pt-loaded WO_3 powder was obtained after a high-temperature treatment at 400°C for 1 hour.

The morphology of the prepared Pt-loaded WO_3 powder was characterized using a field emission scanning electron microscope (FE-SEM, ZEISS Sigma 300) and shown in Figs. 2(a) and (b). Moreover, the elemental analysis of the prepared Pt-loaded WO_3 powder was carried out by energy dispersive spectrometry (EDS, BRUKER XFlash 6130) using an X-ray detector attached to the SEM instrument. As shown in Fig. 2(c), the molar ratio of Pt and WO_3 is controlled at about 3:4 in the prepared Pt-loaded WO_3 powder.

3.2. Fabrication of in-fiber MZI hydrogen sensor

The fabrication process of the in-fiber MZI hydrogen sensor is illustrated in Fig. 3.

In step 1, as shown in Fig. 3(a1), a half-pitch (i.e. a length of 490 µm) of GIF (YOFC, 62.5/125 GIF 0.275) was spliced with two pieces of SMFs (Corning SMF-28), which performed as the two pigtails. In step 2, as shown in Fig. 3(a2), a rectangular-shape air cavity with a length of 80 µm and a width of 30 µm was created in the middle of GIF (i.e., the quarter-pitch position).The

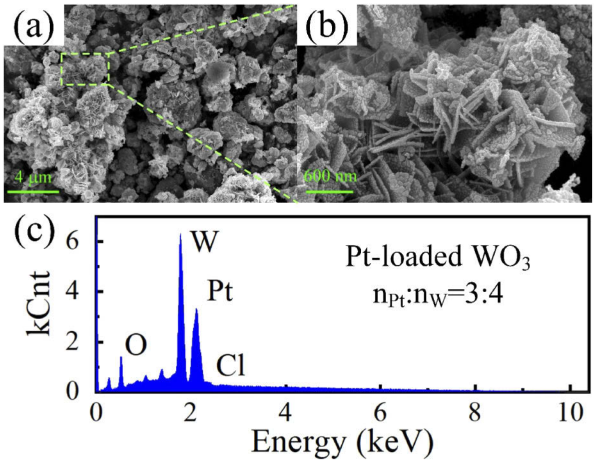

Fig. 2. (a), (b) SEM images of the prepared Pt-loaded WO_3 powder captured in different scales exhibiting the morphologies. (c) Energy dispersive spectrometry (EDS) pattern of the prepared Pt-loaded WO_3 powder.

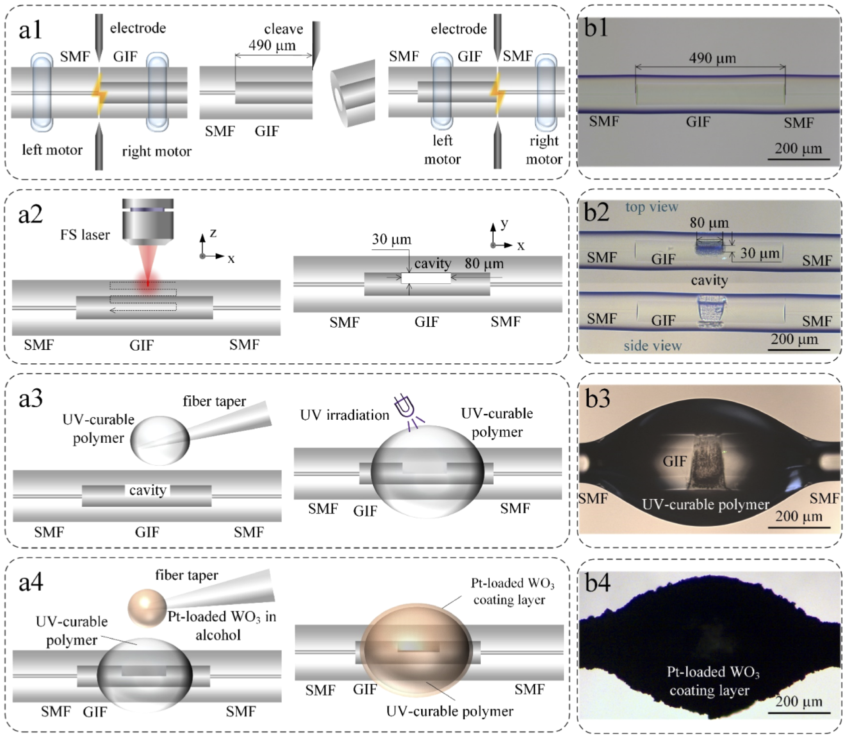

Fig. 3. (a1) - (a4) Schematic diagram of the fabrication process of in-fiber MZI hydrogen sensor: (a1) in step 1, splicing a half-pitch GIF with two SMF pigtails; (a2) in step 2, creating an air cavity inside the GIF core using femtosecond laser ablation; (a3) in step 3, infiltrating the air cavity with UV-curable polymer; (a4) in step 4, coating the polymer-infiltrated MZI with Pt-loaded WO_3 powder. (b1) - (b4) The corresponding microscopic images of an in-fiber MZI hydrogen sensor fabricated after step 1 - 4, respectively.

cavity was fabricated at one lateral side of the GIF core by ablating the silica material using a femtosecond laser (FS laser, Spectra-Physics, 800 nm, 120 fs, 1 kHz, 15 mW). In step 3, as shown in Fig. 3(a3), the air cavity was infiltrated with thermosensitive polymer via a tapered fiber. Commercial UV-curable polymer (NOA 68, RI = 1.540 at room temperature), which has a large thermo-optic coefficient, was used as the thermosensitive polymer. After infiltration, the polymer was cured by UV illumination for 1 hour and annealed at 50°C for 12 hours. Finally, in step 4, as shown in Fig. 3(a4), the prepared Pt-loaded WO_3 powder was dispersed into alcohol, and then dip-coated on the surface of the polymer-infiltrated MZI. The hydrogen sensor was obtained after natural evaporation of the alcohol. Moreover, the corresponding microscopic images of an in-fiber MZI hydrogen sensor fabricated after step 1 - 4, are exhibited in Figs. 3(b1) - (b4), respectively. Obviously, the coated and infiltrated MZI sensor has an ellipsoidal shape. The cross-sectional-view scanning electron microscopic (SEM) images of the fabricated in-fiber MZI hydrogen sensor were acquired, as shown in Fig. 4. Thanks to the strong adhesion of the infiltrated UV-curable polymer, the Pt-loaded WO_3 coating layer could attach firmly to the surface of the polymer-infiltrated in-fiber MZI. In addition, it could also be found in Fig. 4(b) that the thickness of the Pt-loaded WO_3 coating layer is determined as a few micrometers.

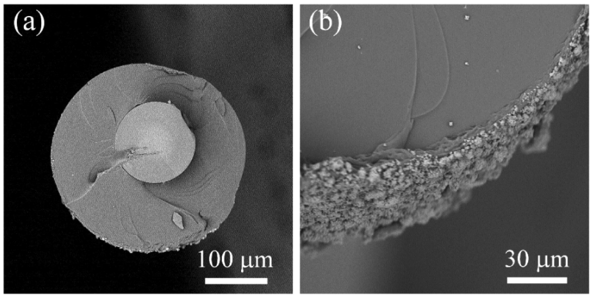

Fig. 4. Cross-sectional-view SEM images of the fabricated in-fiber MZI hydrogen sensor.

4. Experimental results and discussions

4.1. Experimental setup for hydrogen sensing

As shown in Fig. 5, purified H_2 gas was generated from a hydrogen generator (BCHP, TH500), and then sent into the mixing chamber. Meanwhile the air flowed into the mixing chamber by use of an air compressor (Denair, DW65). Two flow meters (Sevenstar, D07-19B and CS200A) were used for precisely controlling the flow rate of H_2 and air, respectively. Consequently, the hydrogen concentration in the mixed gas could be precisely controlled. Moreover, the humility was monitored and controlled via a hygrometer (Rotronic, HygroPalm HP22) and desiccant filled in the mixing chamber. Then, the mixed gas was sent into the air chamber (Ø10 mm × 50 mm), in which the fabricated in-fiber MZI hydrogen sensor was placed. A broadband light source (BBS, FiberLake, wavelength: 1250 ~ 1650 nm, bandwidth: 400 nm) and an optical spectrum analyzer (OSA, Yokogawa, 6370C) were used for recording the transmission spectra of the in-fiber MZI hydrogen sensor under different hydrogen concentrations. And the ambient temperature was controlled to be a constant of 22°C during the hydrogen measurements.

4.2. Response to temperature

The intrinsic temperature response of the in-fiber MZI hydrogen sensor was investigated by use of a high-precision column oven (LCO 102). The temperature was gradually increased from 26°C to 54°C with a step of 4°C. Figure 6(a) demonstrates the evolutions of transmission spectra with

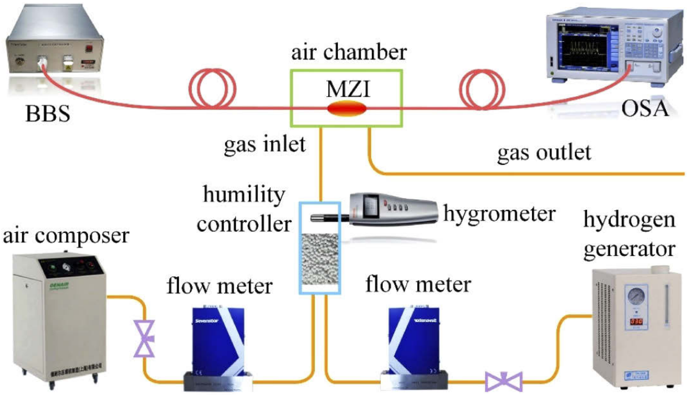

Fig. 5. The schematic diagram of experimental setup for hydrogen detection. BBS: broadband light source, MZI: Mach-Zehnder interferometer, OSA: optical spectrum analyzer, PC: personal computer.

different temperatures. It could be seen the transmission spectrum of the MZI hydrogen sensor exhibits a 'blue shift' with temperature increase. Figure 6(b) demonstrates a linear relationship between the temperature and the resonance dip wavelength. The linear fitting indicates that the MZI has a high temperature sensitivity (-10.40 nm/°C) and a good repeatability.

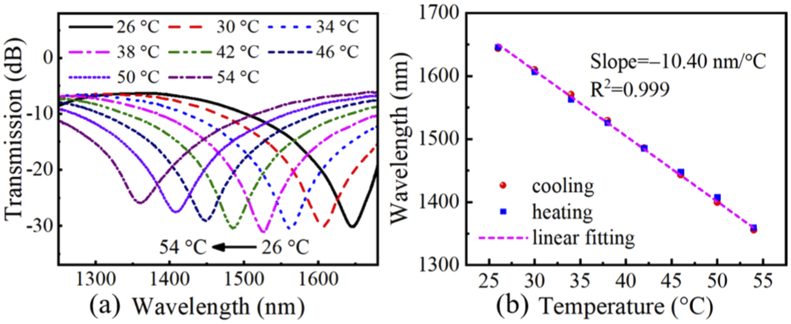

Fig. 6. (a) The transmission spectra evolutions of the polymer- infiltrated MZI with temperature increase. (b) The resonance dip wavelengths as a function of the temperatures.

4.3. *Response to hydrogen*

We studied the hydrogen response of the MZI sensor, which was placed in the air chamber at room temperature, as shown in Fig. 5. The air flow rate was set to 500 stand-state cubic centimeter per minute (sccm). The concentration range was set to 0~0.8% in a step of 0.1%. Figure 7(a) demonstrates the typical transmission spectra evolutions of the MZI sensor with hydrogen concentration changes in the range of 0~0.8%. It is found the resonance dip shifts to shorter wavelengths ('blue' shift), and the maximum wavelength shift of the tracing dip is more than 318 nm. Figure 7(b) demonstrates the wavelength of resonance dip and sensitivity versus hydrogen concentration in the range of 0~0.8%. The hydrogen sensitivity, obtained via calculus of resonant wavelength differences between two adjacent concentration measurement points, exhibits nonlinear variation with the increase of hydrogen concentration. The sensitivity increases up to 1948.68 nm/% at the hydrogen concentration of 0.8%. In contrast to the selectively infiltrated PCF [11], the Fabry-Perot based sensor [13,14], the Sagnac interferometer based-hydrogen sensor

[17], the FBG-based sensor [23], the MZI hydrogen sensor exhibits a much higher sensitivity, resulting from the large thermo-optic coefficient α_P in the UV-curable polymer as described above.

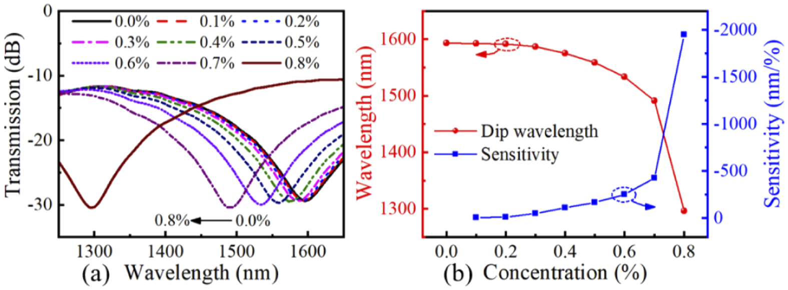

Fig. 7. (a) Transmission spectra evolution of the MZI sensor with various hydrogen concentrations. (b) The resonance dip wavelength and hydrogen sensitivity as functions of hydrogen concentrations.

4.4. Temporal response and repeatability

We studied the real-time response of the MZI sensor to hydrogen. In this experiment, the hydrogen flow rate was changed rapidly between 0% and 0.8% by switching the hydrogen valves, while the air flow rate remained constant (500 sccm). Each step was maintained for ~60 s. As shown in Fig. 8(a), the hydrogen concentration is varied from 0 to 0.8% for several times, the MZI hydrogen sensor exhibits a fast rising and falling response time of ~38 and ~15 s, respectively. Moreover, when hydrogen flows into the gas chamber, the MZI hydrogen sensor takes a quick response to hydrogen, and the tracing dip moves initially quickly, then slowly, and finally approaches to a constant. This phenomenon may result from the chemical reaction-induced temperature difference between the sensor and surrounding medium. When hydrogen exists in the air, Pt-loaded WO_3 catalyzes the reaction of hydrogen with oxygen in accompany with the generation, conduction, and dissipation of heat. At the very beginning, a vigorous chemical reaction takes place and quickly generates a large amount of heat, resulting in a rapid temperature increase and a rapid shift in the resonant wavelength. And then, in case the temperature is further increased, the heat dissipation accelerates, whereas the heating rate is hardly changed, resulting in a slower temperature increase. Subsequently, in case the heat production rate and heat dissipation rate are in equilibrium, the resonant wavelength reaches a constant. Hence, it takes a longer rising response time of ~38 s to reach the equilibrium in the hydrogen concentration increasing process. However, when the hydrogen flow is turned off and the hydrogen concentration is lowered down to zero. In this situation, heat production no longer exists and the air flow takes the heat away quickly, showing a shorter falling response time of ~15 s to reach the equilibrium in the hydrogen concentration decreasing process. The hydrogenation cycling was repeated, and the reactions are almost the same as the first one. In addition, the repeatability of the proposed MZI hydrogen sensor was studied when the hydrogen concentration was increased from 0 to 0.8% with a step of 0.2% for three times. As shown in Fig. 8(b), the sensor has similar wavelength shifts with the same hydrogen concentration, exhibiting an excellent repeatability.

4.5. Flow rate influence

To explore the influence of the gas flow rates on the MZI hydrogen senor, sample 1 and 2 were tested and the results are shown in Fig. 9. As shown in the insets of Figs. 9(a) and (b), sample 1 has a width of 691 μm and a height of 424 μm, whereas sample 2 has a width of 1350 μm and a height of 942 μm, i.e., sample 2 is nearly twice larger in size than sample 1. For sample 1, as

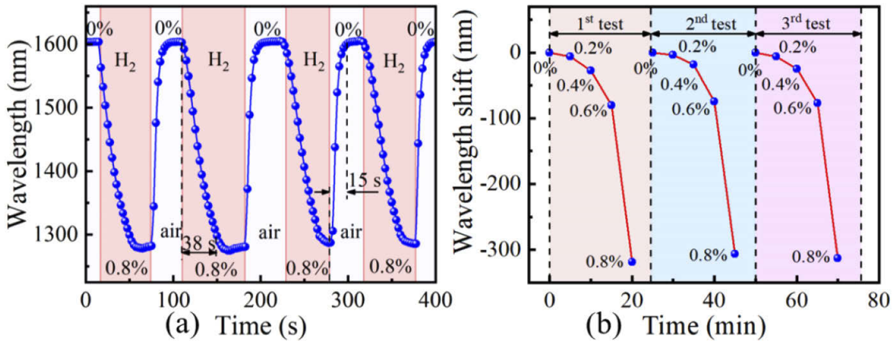

Fig. 8. (a) Resonant dip wavelength of the hydrogen sensor in successive hydrogenation cycles (switched from 0% to 0.8%, vol %). (b) Wavelength shift of the hydrogen sensor in three repeated tests.

shown in Fig. 9(a), the changes take place as the flow rates increase from 200 sccm to 300 sccm. When the flow rate is higher than 300 sccm, the wavelength shifts under different flow rates (300, 400, 500 sccm) are almost the same. As shown in Fig. 9(b), similar results were also discovered in sample 2. As the flow rate increases, more hydrogen molecules could collide with the sensitive layer per second, producing more heat. On the other hand, in case of a higher flow rate, heat will be taken away faster from the sensor. As the flow rate increases and the concentration is larger than 0.9%, the hydrogen sensitivity of sample 2 slightly increases at first, and then reaches the maximum at the flow rate of 300 sccm. Thus, it is obvious that a smaller sensor size can lead to an increase in hydrogen sensitivity.

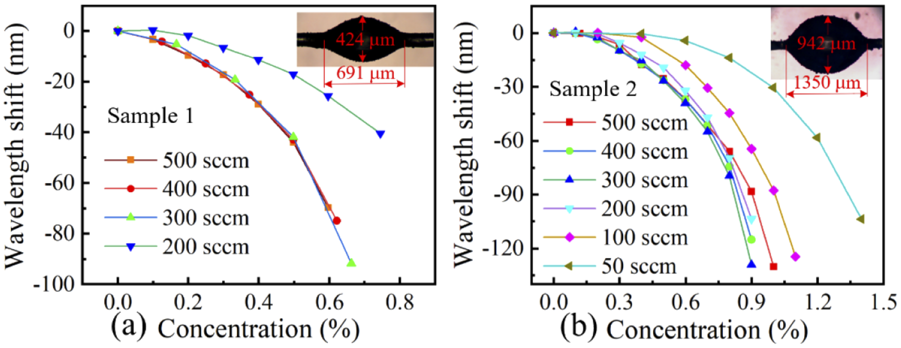

Fig. 9. Wavelength shift as functions of hydrogen concentrations with various flow rates applied on sample 1 (a) and 2 (b), which have different sensor sizes.

4.6. Humidity influence

Finally, the influence of relative humidity on the stability of the proposed hydrogen sensor was investigated. Four types of air with different relative humidity were adopted by putting desiccant or wet tissue into the mixing chamber. Figure 10(a) shows the hydrogen response of the proposed sensor under different relative humidity. In case the proposed sensor was tested in a dry atmosphere with a relative humidity of 6.1%, the sensor exhibits a maximum wavelength shift of ~145 nm at a hydrogen concentration of 0.6%. In case the relative humidity is increased to a higher value of 33.8%, the wavelength exhibits a smaller shift of ~60 nm at the same hydrogen concentration of 0.6%. Moreover, in case the relative humidity is further increased to higher values above 33.8%, the wavelength seems to be irrelevant to humidity. Figure 10(b) shows the temporal response of the proposed sensor in a hydrogen concentration of 0.6%. The proposed sensor has a response time of ~57 s with a relative humidity of 6.1% in atmosphere, whereas when the relative humidity is larger than 33.8%, the response time has the same value of ~32 s. These results may be induced by the increase in heat exchange between the sensor and the air with a relatively low humidity, and the humidity influence on the heat exchange would be saturated with a relatively higher humidity.

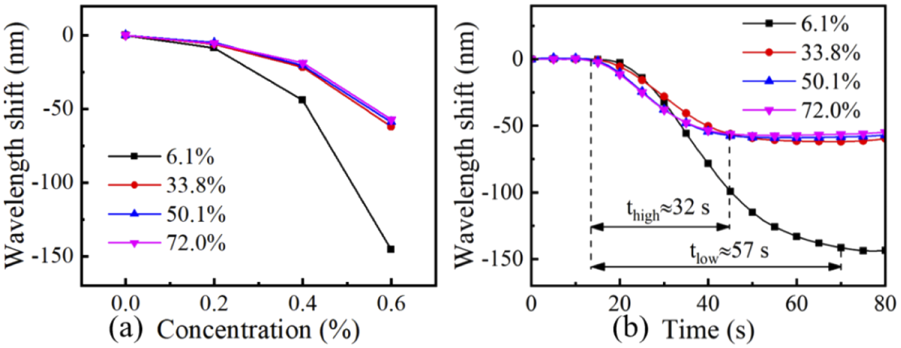

Fig. 10. (a) Wavelength shifts as functions of hydrogen concentrations in air with different relative humidity. (b) Temporal responses in air with different relative humidity.

4.7. Discussion

Table 1 displays some typical results from previously reported optical fiber hydrogen sensors. Compared with other types of hydrogen sensors, the MZI hydrogen sensor proposed in this work has the largest sensitivity, a fast response, and a strong robustness. Nevertheless, the MZI hydrogen sensor exhibits a relatively small hydrogen concentration range, which is partially limited by the operation range of OSA. This shortcoming could be solved by using either an OSA with a wider operation range or a high-resolution intensity demodulation scheme. Furthermore, the hydrogen sensing of the proposed MZI hydrogen sensor is based on the detection of heat generated in the coated Pt-loaded WO_3. The infiltrated polymer material in the cavity is also quite sensitive to temperature. Hence, in order to eliminate the influence of ambient temperature fluctuations on the hydrogen measurement, we may use two cascaded polymer-infiltrated MZI sensors, i.e., one MZI coated with Pt-loaded WO_3 used for hydrogen sensing and the other uncoated MZI used for temperature compensation.

Table 1. Comparison of the optical fiber hydrogen sensors' performance

Structure	Concentration Range	Sensitivity	Response Time	Reference
Selectively infiltrated PCF	1~4%	32.3 nm/%	102 s	[11]
PANDA PMF	0~1%	7.877 nm/%	<100 s	[17]
Double C cavity	0~1%	15.14 nm/%	~23 s	[12]
Cascaded FPI	0~2.4%	−1.04 nm/%	~80 s	[13]
polymer-filled FPI	0–4.0%	17.48 nm/%	<30 s	[14]
Sagnac interferometer loop	0%-0.8%	−14.61 nm/%	n/a	[15]
Polymer infiltrated MZI	0~0.8%	−1948.679 nm/%	~38 s	this work

5. Conclusion

We proposed a fiber MZI sensor for highly sensitive hydrogen sensing. A half-pitch GIF used in the MZI can enlarge the waist radius, and hence can decrease the transmission loss and the precision requirement in the cavity ablating process. The utilization of UV-curable polymer filled in the MZI can induce a high temperature sensitivity of ~10.40 nm/°C. The exothermic reaction provided by the coating layer makes it sensitive to the hydrogen, and the sensitivity increases from -7.09 to -1948.679 nm/% with a rising response time of 38 s and falling response time of ~15 s, respectively, in a hydrogen concentration ranges of 0~0.8%. The advantages of robustness, accuracy, good repeatability, make the proposed MZI sensor promising for trace hydrogen leakage monitoring in many applications, such as safety production and hydrogen medical research.

Funding. National Natural Science Foundation of China (61875128, U1913212, 91860138); Guangdong Science and Technology Department (2019TQ05X113, 2019A050510047, 2019A1515011393); Science, Technology and Innovation Commission of Shenzhen Municipality (JCYJ20180507182058432, JCYJ20180305125352956).

Disclosures. The authors declare no conflicts of interest.

References

1. M. Tabib-Azar, B. Sutapun, R. Petrick, and A. Kazemi, "Highly sensitive hydrogen sensors using palladium coated fiber optics with exposed cores and evanescent field interactions," Sens. Actuators, B **56**(1-2), 158–163 (1999).
2. D. A. Crowl and Y. Jo, "The hazards and risks of hydrogen," J. Loss Prevent. Proc. **20**(2), 158–164 (2007).
3. M. Wang, D. N. Wang, M. Yang, J. Cheng, and J. Li, "In-line Mach-Zehnder Interferometer and FBG with Pd film for simultaneous hydrogen and temperature detection," Sens. Actuators, B **202**, 893–896 (2014).
4. F. Gu, G. Wu, and H. Zeng, "Hybrid photon–plasmon Mach–Zehnder interferometers for highly sensitive hydrogen sensing," Nanoscale **7**(3), 924–929 (2015).
5. M. Wang, M. Yang, J. Cheng, G. Zhang, C. R. Liao, and D. N. Wang, "Fabry–Pérot interferometer sensor fabricated by femtosecond laser for hydrogen sensing," IEEE Photonics Technol. Lett. **25**(8), 713–716 (2013).
6. C. Ma and A. Wang, "Optical fiber tip acoustic resonator for hydrogen sensing," Opt. Lett. **35**(12), 2043–2045 (2010).
7. J. Dai, M. Yang, Y. Chen, K. Cao, H. Liao, and P. Zhang, "Side-polished fiber Bragg grating hydrogen sensor with WO_3-Pd composite film as sensing materials," Opt. Express **19**(7), 6141–6148 (2011).
8. A. Hosoki, M. Nishiyama, H. Igawa, A. Seki, and K. Watanabe, "A hydrogen curing effect on surface plasmon resonance fiber optic hydrogen sensors using an annealed Au/Ta_2O_5/Pd multi-layers film," Opt. Express **22**(15), 18556–18563 (2014).
9. S. Cai, A. Gonzalez-Vila, X. Zhang, T. Guo, and C. Caucheteur, "Palladium-coated plasmonic optical fiber gratings for hydrogen detection," Opt. Lett. **44**(18), 4483–4486 (2019).
10. M. Yang, Z. Yang, J. Dai, and D. Zhang, "Fiber optic hydrogen sensors with sol–gel WO_3 coatings," Sens. Actuators, B **166-167**, 632–636 (2012).
11. Y. Wang, D. Wang, F. Yang, Z. Li, and M. Yang, "Sensitive hydrogen sensor based on selectively infiltrated photonic crystal fiber with Pt-loaded WO_3 coating," Opt. Lett. **39**(13), 3872–3875 (2014).
12. Y. Li, W. Shen, C. Zhao, B. Xu, D. Wang, and M. Yang, "Optical hydrogen sensor based on PDMS-formed double-C type cavities with embedded Pt-loaded WO_3/SiO_2," Sens. Actuators, B **276**, 23–30 (2018).
13. Y. Li, C. Zhao, B. Xu, D. Wang, and M. Yang, "Optical cascaded Fabry–Perot interferometer hydrogen sensor based on vernier effect," Opt. Commun. **414**, 166–171 (2018).
14. B. Xu, P. Li, D. Wang, C. Zhao, J. Dai, and M. Yang, "Hydrogen sensor based on polymer-filled hollow core fiber with Pt-loaded WO_3/SiO_2 coating," Sens. Actuators, B **245**, 516–523 (2017).
15. B. Wu, C. Zhao, B. Xu, and Y. Li, "Optical fiber hydrogen sensor with single Sagnac interferometer loop based on vernier effect," Sens. Actuators, B **255**, 3011–3016 (2018).
16. Y. Zhang, H. Peng, X. Qian, Y. Zhang, G. An, and Y. Zhao, "Recent advancements in optical fiber hydrogen sensors," Sens. Actuators, B **244**, 393–416 (2017).
17. B. Xu, C. Zhao, F. Yang, H. Gong, D. Wang, J. Dai, and M. Yang, "Sagnac interferometer hydrogen sensor based on panda fiber with Pt-loaded WO_3/SiO_2 coating," Opt. Lett. **41**(7), 1594–1597 (2016).
18. F. Zhang, X. Xu, J. He, B. Du, and Y. Wang, "Highly sensitive temperature sensor based on a polymer-infiltrated Mach–Zehnder interferometer created in graded index fiber," Opt. Lett. **44**(10), 2466–2469 (2019).
19. X. Xu, J. He, M. Hou, S. Liu, Z. Bai, Y. Wang, C. Liao, Z. Ouyang, and Y. Wang, "A miniature fiber collimator for highly sensitive bend measurements," J. Lightwave Technol. **36**(14), 2827–2833 (2018).
20. B. Du, X. Xu, J. He, K. Guo, W. Huang, F. Zhang, M. Zhang, and Y. Wang, "In-fiber collimator-based Fabry-Perot interferometer with enhanced vibration sensitivity," Sensors **19**(2), 435 (2019).
21. O. Arrizabalaga, G. Durana, J. Zubia, and J. Villatoro, "Accurate microthermometer based on off center polymer caps onto optical fiber tips," Sens. Actuators, B **272**, 612–617 (2018).

22. H. Gao, Y. Jiang, Y. Cui, L. Zhang, J. Jia, and L. Jiang, “Investigation on the thermo-optic coefficient of silica fiber within a wide temperature range,” J. Lightwave Technol. **36**(24), 5881–5886 (2018).
23. X. Zhou, Y. Dai, J. M. Karanja, F. Liu, and M. Yang, “Microstructured FBG hydrogen sensor based on Pt-loaded WO_3,” Opt. Express **25**(8), 8777–8786 (2017).